热镀锌高强钢点焊的电极磨损机理分析

张旭强[1]，　张延松[2]，　陈关龙[2]

（1. 中国石油大学(华东) 机电工程学院，山东 东营　257061；
2. 上海交通大学 机械与动力工程学院，上海　200030）

摘　要：热镀锌高强钢点焊的电极端面合金化作用机制复杂、电极磨损严重. 进行磨损电极的元素成分与金相试验分析，研究电极端面合金化作用机制与微观组织演变规律，揭示其电极磨损机理. 结果表明，在合金层中发现镀层中的Zn，Al 元素，锌、铝与铜在不同温度与含量情况下形成不同相合金，使电极端面导电、导热能力变差，镀层中铝的存在是电极磨损严重的一个主要原因. 电极端面的点蚀区域由于较高的温度与压力作用，很容易产生微裂纹，熔化的镀锌层金属元素沿微裂纹渗入电极内部，加速电极失效. 电极再结晶区域发生组织再结晶，由柱状晶转变为等轴晶，使电极硬度降低，抗塑性变形能力变差.

关键词：电极磨损；热镀锌高强钢；合金化；电阻点焊
中图分类号：TG455　　文献标识码：A　　文章编号：0253－360X(2009)11－0041－03

张旭强

0　序　　言

热镀锌高强钢由于高强度特性与良好的抗腐蚀性，可满足汽车轻量化与安全性的需要，在车身制造中逐渐得到广泛应用. 但热镀锌高强钢点焊的工艺性差，电极磨损严重，电极寿命远远低于非镀层低碳钢板[1,2]. 镀锌层与电极端面合金化作用机制复杂，其电极磨损机理须进一步研究. 文中以热镀锌高强钢为研究对象，试验研究热镀锌高强钢点焊的电极端面与镀锌层合金化作用机制及其微观组织演变规律，揭示热镀锌高强钢点焊的电极磨损机理.

1　试验方法

电阻点焊中，电极在高温、高压作用下与工件频繁接触，工作条件十分恶劣. 点焊镀锌板、铝合金等材料时电极头部温度可高达 800～900 ℃[3]，电极端部反复受热、受压，极易变形失效. 因而要求电极具有良好的导电、导热能力以及较高的强度与抗氧化能力. 试验所采用的电极是端面直径为 5 mm 的球形电极，电极材料为铬(Cr：0.7%)锆(Zr：0.1%)铜电极. 试验采用的焊件材料是强度为 600 MPa、厚度为 1.5 mm 的热镀锌高强钢，焊件主要成分与焊枪类型详见文献[1]. 焊枪首先在大样件上进行电极磨损试验，大样件尺寸为 500 mm×100 mm×1.5 mm，焊点间距为 20 mm. 磨损试验的具体焊接工艺参数如表 1 所示. 每隔 100 点利用小样件采集焊点试样，用于拉剪试验，小样件尺寸为 100 mm×40 mm×1.5 mm. 电极磨损试验以焊点拉剪力有明显下降且未形成熔核为结束标志. 共进行 3 组电极磨损试验，获取不同磨损状态下的电极试验样本，进行电极金相试验分析.

表 1　电极磨损试验焊接工艺参数

Table 1　Welding parameters of electrode wear

预压时间 t_y/s	焊接时间 t_h/s	保持时间 t_b/s
0.24	0.36	0.12
电极力 F/N	焊接电流 I/kA	冷却水流量 q/(L·min^{-1})
4 300	11	8.0

2　试验结果与分析

2.1　电极端面合金化

点焊热镀锌高强钢时，镀层中的金属元素与铜电极在高温高压下极易发生合金化反应，随着电极磨损的加剧，在电极端面形成导电、导热能力差的合金层. 为分析合金层区域的金属成分变化，采集不同焊接点数下的磨损电极样本，沿电极轴向方向剖

收稿日期：2008－07－22
基金项目：国家自然科学基金资助项目(50575140)

开,经过打磨、腐蚀等工艺处理,制成电极金相样本,进行电镜扫描与元素成分分析(SEM /EDS). 电极合金层区域的 SEM 照片如图 1 所示,左边区域(图中 5 号位置)为铜电极内部本体区域,向右经过合金层区域逐步过渡到电极端面.

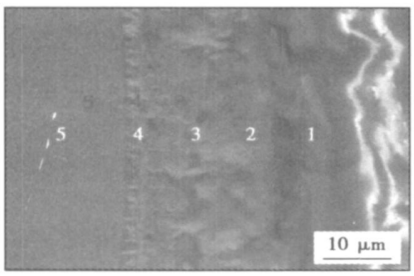

图 1 电极合金层 SEM 形貌

Fig. 1 Analysis of SEM in alloying layer

根据图 1 所示的合金层区域不同点的位置,自电极本体内部至电极端面不同位置进行金属元素成分分析(EDS 分析). 在铜电极内部(5 号区域)发现的元素成分主要为 Cu,而合金层区域(2 号区域)除了 Cu 元素之外,还发现 Zn, Al, Fe 等金属元素. 在合金层不同位置,利用 EDS 分析得到磨损电极各金属元素摩尔分数随测试点位置的变化规律如图 2 所示,其中 C, O, Si 等元素的含量由于与合金层的形成没有关系,没有列入统计分析.

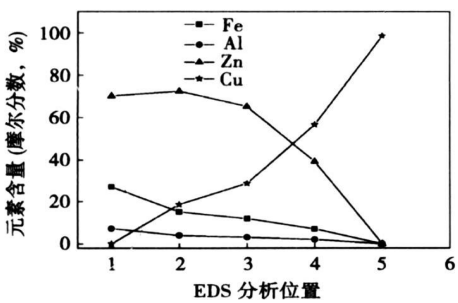

图 2 合金层区域不同测试位置金属元素成分及含量

Fig. 2 Elements at different alloying regions

从图 2 的统计分析可以看出 Zn 元素摩尔分数随着分析位置向电极内部移动而逐渐减少,Cu 元素含量则相应增加. 此外,合金层中还有一定量的 Al, Fe 元素. 在电极端面,Fe 元素在高温高压下通过扩散作用进入合金层,使电极端面的 Fe 元素摩尔分数较高. 由于相近的材料属性,锌与铜在高温下的相互扩散能力比较强. 随着 Zn, Cu 元素含量的变化,在不同温度下可以形成一系列 α, β, γ 等相合金[4],这些相合金易脆、导电导热能力差、高温下抗塑性变形能力较差[3],加速了电极的磨损.

从 EDS 分析结果中可以发现合金层里含有一定量的 Al 元素. 铝的密度小、熔点与强度低,与铜的合金化倾向较强. 当铝、铜异种金属以固态/液态或液态/液态相互接触时,发生物理化学作用. 物理作用的结果主要就是粘附,化学作用主要是金属之间的合金化,其结果主要是生成固溶体与金属间化合物. 从 Cu, Al 元素二元相图可以看出,在不同的摩尔分数下,铜与铝之间依次可以形成铝的 α 固溶体、θ 相($CuAl_2$ 为基的固溶体)、铜的 α 固溶体和中间相. 由于铝在铜中的扩散速率远远高于锌在铜中的扩散速率,使铝与铜更易于合金化,镀层中铝的含量越高,电极磨损越快. 铝与铜的合金化速度快于锌与铜的合金化速度,这种合金化加快了电极端面直径磨损,并且电极端面的铝合金产物具有易脆性,很容易脱落,使露出的 Zn-Cu 合金进一步发生合金化,加剧了电极的磨损.

图 3 为磨损电极的金相试验样本,从图 3 中可以看出,电极端面发生点蚀,且点蚀部位伴有微裂纹产生. 点焊时点蚀区域的温度较高,点蚀边缘容易产生应力集中,因而在点蚀区域很容易产生微裂纹. 裂纹末端渗入电极内部的微观组织形貌如图 4 所示,对图 4 中微裂纹区域进行 EDS 分析,结果发现微裂纹区域含有大量的 Zn, Al 等镀层中的金属元素,即工件镀层中的金属熔化后,顺着微裂纹渗入电极内部,微裂纹在镀层元素作用下进一步扩大,加速电极失效.

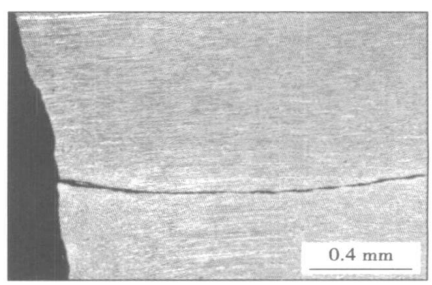

图 3 磨损电极金相试验样本

Fig. 3 Metallographic specimen of worn electrode

2.2 电极端面微观组织演变规律

根据磨损电极微观组织变化特点,自电极端面沿电极轴线向电极本体内部方向,可将电极组织变化分为三个区域. 磨损电极金相样本的微观组织形貌如图 5 所示,自左向右依次为端面合金层区域、再

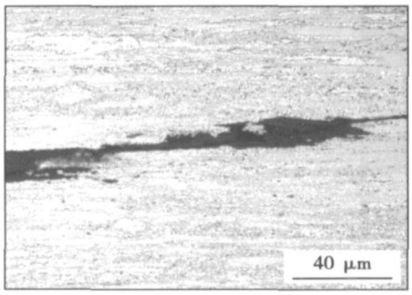

图 4　裂纹末端渗入电极内部的微观组织形貌

Fig. 4　Micro-structure at end of crack in electrode

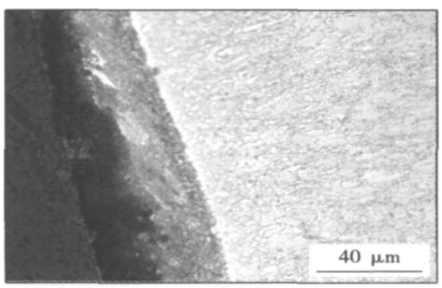

图 5　磨损电极微观组织形貌

Fig. 5　Micro-structure of worn electrode

结晶区域以及电极内部区域.

电极本体内部区域与再结晶区域的微观组织形貌如图 6 和图 7 所示，从图中可以看出再结晶区域组织与铜电极本体组织有明显的不同，电极本体内部主要是柱状晶组织. 再结晶区域靠近电极端面，点焊时该区域温度比较高，在反复高温、高压作用下，该区域组织发生再结晶，由柱状晶转变为等轴晶. 相比较于柱状晶组织，等轴晶组织强度、硬度比较低，使再结晶区域强度与硬度降低.

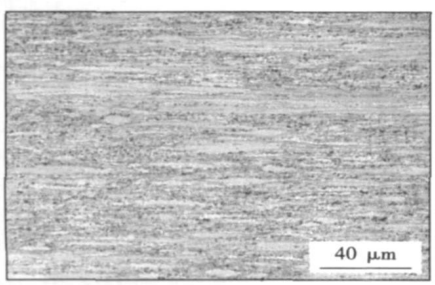

图 6　电极内部本体微观组织形貌

Fig. 6　Micro-structure in inner electrode

进行磨损电极微观硬度测试(维氏硬度)，以分析合金层微观组织变化对电极硬度的影响. 硬度测试从发生合金化的电极端面开始，沿电极轴线向电极内部移动. 在电极中心轴线以及距离电极边缘各 0.5 mm 的部位进行 3 组硬度测量试验. 维氏硬度测试的载荷为 2 N，保压时间为 15 s. 磨损电极在不同位置的硬度测试结果如图 8 所示，距离电极端面较近的部位硬度较低，电极内部区域硬度较高. 原因主要是在电、热、力的耦合作用下，电极端面区域发生合金化与组织再结晶，使电极软化，硬度降低. 金属材料的屈服应力与其硬度成正比关系[5]. 硬度测试结果表明，电极端面的合金层与再结晶使电极硬度降低，因而电极屈服应力也相应降低，使电极抗塑性变形能力变差，加速电极失效.

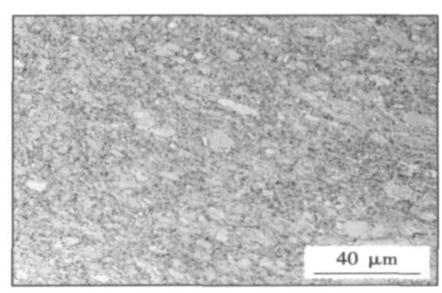

图 7　电极再结晶区域微观组织形貌

Fig. 7　Micro-structure in recrystallization region

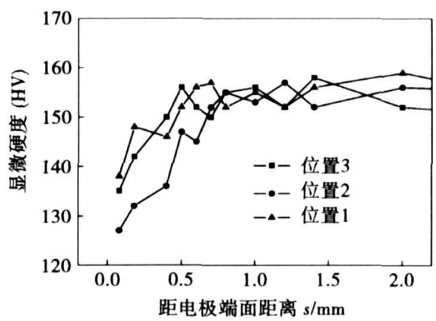

图 8　磨损电极硬度随测试位置的变化曲线

Fig. 8　HV of worn electrodes at different positions

3　结　　论

(1) 在磨损电极合金层中发现工件镀层中的 Zn，Al 等元素. Zn 元素的摩尔分数随分析位置向电极内部移动逐渐减少，Cu 元素摩尔分数则相应增加. 在不同的温度下，随着 Zn，Cu 元素含量的变化，可形成不同的相合金，铝与铜的合金化作用加剧电极磨损. 所形成合金层的强度较低、易脆、高温下抗

[下转第 48 页]

高, APS 喷涂时粒子和涂层氧化较为严重, 铝的损耗更多, 所以 SAPS 涂层在 1 080 ℃表现出比 APS 更好的抗高温氧化能力.

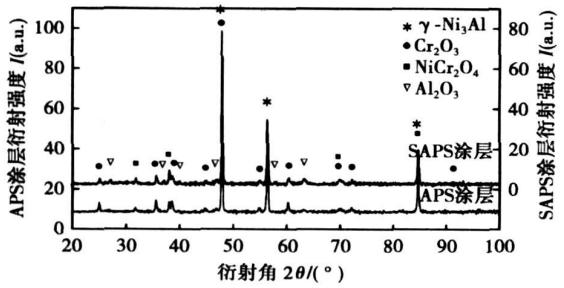

图 7 SAPS 和 APS 涂层在 1 080 ℃氧化 24 h 后 XRD 衍射图

Fig. 7 XRD patterns of SAPS and APS coatings after 1 080 ℃ for 24 h

3 结 论

(1) 对于大气等离子喷涂而言, 涂层的氧化主要取决于粒子飞行中的氧化和涂层形成过程中的氧化. 在其它喷涂工艺参数确定的情况下, 粒子飞行中的氧化主要取决于粒子的飞行距离, 飞行的距离越长, 粒子的氧化程度越大; 喷涂材料的性质对粒子和涂层的氧化程度有明显影响, 相比较喷涂铁粉时粒子和涂层的氧化程度要远大于 NiCoCrAlY 粉.

(2) 粒子的氧化形式与粒子距喷嘴距离有关. 在距离喷嘴一定距离(45 mm)以内的等离子射流中心处, 粒子的氧化形式以对流氧化为主, 在这个距离以远的后半段, 粒子的氧化形式将以扩散氧化为主.

(3) 采用附加氩气保护罩可减少等离子射流中混入的空气量, 能明显降低粒子和涂层的 O 元素含量.

(4) 粒子的氧化程度和涂层氧化物夹杂的多少会影响扁平粒子铺展, 从而会影响涂层的孔隙率. 粒子和涂层氧化程度增加会使涂层的孔隙率增加, 合金元素烧损增多, 抗高温氧化能力下降.

参考文献:

[1] Pant B K, Arya V, Mann B S. Development of low-oxide MCrAlY coatings for gas tribune applications[J]. Journal of Thermal Spray Technology, 2007, 16(2): 275—280.

[2] Brandl W, Toma D, Kruger J, *et al*. The oxidation behavior of HVOF thermal-sprayed MCrAlY coatings[J]. Surface and Coatings Technology, 1997, 94/95: 21—26.

[3] Volenik K, Leitner J, Hanousek F, *et al*. Oxides in plasma-sprayed chromium steel[J]. Thermal Spray Technology, 1997, 6(3): 327—334.

[4] Syed A A, Denoirjean A, Fauchais P, *et al*. On the oxidation of stainless steel particles in the plasma jet[J]. Surface and Coatings Technology, 2006, 200(14—15): 4368—4382.

[5] Deshpande S, Sampath S, Zhang H, *et al*. Mechanisms of oxidation and its role in microstructure evolution of metallic thermal spray coatings—case study for Ni-Al[J]. Surface and Coatings Technology, 2006, 200(18—19): 5395—5406.

[6] Kolmen D, Volenik K. Modeling of oxidation during plasma spraying of iron particles[J]. Plasma Chemistry and Plasma Processing, 2002, 22(3): 437—450.

[7] Xu H B, Gong S K, Deng L. Preparation of TBCs for gas turbine blades by EB-PVD[J]. Thin Solid Films, 1998, 334(1—2): 98—102.

[8] Planche M P, Liao H, Coddet C. Oxidation control in atmospheric plasma sparying coating[J]. Surface and Coatings Technology, 2007, 202(1): 69—76.

作者简介: 魏 琪, 男, 1953 年出生, 硕士, 副教授. 主要从事焊接和表面工程研究工作. 发表论文 60 余篇.

Email: weiqi@bjut.edu.cn

[上接第 43 页]

塑性变形能力差.

(2) 热镀锌高强钢点焊的电极端面由于合金化作用产生点蚀. 点蚀区域在高温高压下容易产生微裂纹, 镀层中的金属元素沿微裂纹渗入电极内部, 加速电极失效.

(3) 电极端面发生组织再结晶, 再结晶区域组织由柱状晶转变为等轴晶, 使该区域电极硬度降低, 抗塑性变形能力变差.

参考文献:

[1] 张旭强, 罗爱辉, 张延松, 等. 点焊热镀锌双相高强度钢的电极磨损规律[J]. 焊接学报, 2006, 27(9): 108—112.
Zhang Xuqiang, Luo Aihui, Zhang Yansong, *et al*. Characteristics of electrode wear in spot welding of hot galvanized dual-phase high strength steel[J]. Transactions of the China Welding Institution, 2006, 27(9): 108—112.

[2] 张旭强. 热镀锌高强钢电阻点焊的电极磨损机理与评价研究[D]. 上海: 上海交通大学, 2007.

[3] Fukumoto S, Lum I. Effects of electrode degradation on electrode life in resistance spot welding of aluminum alloy 5182[J]. Welding Journal, 2003, 9(11): 307s—312s.

[4] Massalsk T B. Binary alloys phase diagrams[M]. Ohio: ASM international, 1990.

[5] Zhou M, Zhang H. Critical specimen sizes for tensile shear tests[J]. Welding Journal, 1999, 11(9): 304s—313s.

作者简介: 张旭强, 男, 1974 年出生, 博士, 讲师. 主要研究方向为车身焊接装配质量检测与控制. 发表论文 10 余篇.

Email: zhangxuqiang@163.com

metal. In addition, the welded joint by the fiber laser-MIG hybrid welding has higher Erichsen values than that by laser joints. The difference in plasticity is attributed to the microstructure changes in the welded joint of hybrid welding. Thus, the fiber laser-MIG hybrid welding of CP-Ti can be carried out successfully at higher welding speed with a good combination of weld bead appearance and plasticity.

Key words: fiber laser welding; fiber laser-MIG hybrid welding; titanium alloys; tensile test

Experimental analysis on friction hydro pillar processing of cylindrical coupling of 2024 aluminum alloy CHEN Zhonghai, CHEN Jiaqing, JIAO Xiangdong, ZHOU Canfeng (Research Centre of Offshore Engineering Joining Technology, Beijing Institute of Petrochemical Technology, Beijing 102617, China). p 37—40

Abstract: The cylindrical coupling of 2024 Aluminum alloy was welded by friction hydro pillar processing (FHPP) in the first domestic friction stitch welding machine. The diameter of the consumed metal stud is 14 mm, the depth and diameter of the predrilled hole are 25 mm and 16 mm respectively. The effects of rotational speed and shielding gas on the FHPP quality were mainly studied, and the microstructure and its properties of the sample were analyzed by means of some measuring apparatus such as optical microscope and microhardness tester etc. The results indicate that the low rotation can form the insufficient bonding, even result in the cease of the weld head motor during the welding. The quality of welded joint is better when the rotational speed is 5 000 r/min and the feeding rate is 0.5 mm/s. The shielding gas can improve the quality of FHPP with thinner fusion line, and the upper part of the metal stud is bonded to the base metal very well.

Key words: friction hydro pillar processing; friction stitch welding; 2024 aluminum alloy; microstructure; shielding gas

Experimental study on electrode wear mechanism in resistance spot welding of high strength hot galvanization steels ZHANG Xuqiang[1], ZHANG Yansong[2], CHEN Guanlong[2] (1. School of Mechanical Engineering, Petroleum University of China, Dongying 257061, Shandong, China; 2. School of Mechanical Engineering, Shanghai Jiaotong University, Shanghai 200030, China). p 41—43, 48

Abstract: Surface alloying mechanism on the electrode end face was complex and its wear was serious in welding of high strength hot galvanization steel. Elements composition and metallography experiment of the worn electrode were carried out to study the alloying on electrode end surface and microstructure evolvement. It was shown that the elements of Al, Zn etc were found in alloying layer. Different alloys were formed for different contents of Al, Zn at different temperatures, which decreased conductivity and heat conduction on electrode face. Al in coating was one of the main reasons that led to serious electrode wear. Pitting was grown obviously and micro cracks were produced at pitting region for higher temperature and pressure, the molten metal in coating penetrated into the electrode interior and accelerated electrode invalidation. The metal structure in recrystallization region was changed from columnar crystal to equiaxed crystal, which decreased hardness and anti-plastic deformation capability of electrode.

Key words: electrode wear; high strength hot galvanization steel; alloying; resistance spot welding

Oxidation of metallic particle and its effect on properties of plasma sprayed coatings WEI Qi, ZHANG Linwei, LI Hui, CUI Li (College of Materials Science and Engineering, Beijing University of Technology, Beijing 100124, China). p 44—48

Abstract: The oxidation mechanisms of iron particles and NiCoCrAlY particles during plasma spraying process and its effect on the sprayed coatings were investigated by the in-flight particles collection setup and the gas shrouding. The results show that there are two oxidation mechanisms during in-flight oxidation: one is the diffusion oxidation; the other is the convective oxidation, which are decided by the distance from the spraying particles to the nozzle. The oxidation content increases with the increasing of the standoff distance. The shrouded gas can decrease the oxidation content of in-flight particles and increase the oxidation resistance of NiCoCrAlY coatings.

Key words: plasma spraying; metallic particle; oxidation mechanism; oxidation resistance.

Numerical simulation of welding arc and surface-activating element on weld shape in TIG welding DONG Wenchao, LU Shanping, LI Dianzhong, LI Yiyi (Shenyang National Laboratory for Materials Sciences, Institute of Metal Research, Chinese Academy of Sciences, Shenyang 110016, China). p 49—52, 56

Abstract: Welding arc and weld pool models were established by FLUENT software for spot and moving TIG welding of SUS304 stainless steel to investigate the effect of the surface-activating element oxygen on the weld shape and analyze the properties of argon arc and helium arc and their effects on the weld shape. The results show that the change of the Marangoni convection induced by different oxygen contents can be considered as one of the principal factors to increase penetration. The plasma drag force from the argon arc has obvious effect on the weld shape. Compared with the argon arc, the helium arc is more constricted, the welding current density is much greater and the much more heat flux is transferred into the weld pool, which increase the inward convection induced by the electromagnetic force, thus the deeper weld depth can be obtained. The calculated weld D/W ratio agrees with that of the experiment.

Key words: weld shape; welding arc; surface-activating element; numerical simulation

IMC of SAC0307-*x*Ni/Ni soldered joint and consumption of Ni coating WANG Lingling, SUN Fenglian, WANG Lifeng, ZHAO Zhili (School of Materials Science & Engineering, Harbin University of Science and Technology, Harbin 150040, China). p 53—56

Abstract: The microstructure of interfacial IMC and the consumption of Ni layer for SAC0307/Ni (Sn-0.3Ag-0.7Cu/Ni) soldered joint and SAC0307-0.05Ni/Ni (Sn-0.3Ag-0.7Cu-0.05Ni/Ni) soldered joint after aging at 180 ℃ were studied by scanning electron microscope (SEM). The results indicated that the IMC layer of SAC0307/Ni and SAC0307-0.05Ni/Ni are both $(Cu_{1-x}Ni_x)_6Sn_5$ after reflow soldering. With the increasing of aging time, the thickness of IMC layer increases gradually, the type of IMC is not changed, but the chemical composition changes. The morphology of IMC is storm-